Optical properties of highly scattering media determined from changes in attenuation, phase, and modulation depth

Matthias Kohl, Russell Watson, and Mark Cope

The optical properties of scattering media determine the attenuation (A) and the transit time ($\langle t \rangle$) of light reflected from the medium as well as the phase (Φ) and modulation depth (M) of an intensity-modulated lightwave. Our primary finding is that the ratio of changes in A, Φ, and M is approximately independent of the scattering properties and gives a good estimate of the absorption coefficient. These changes can be induced either by small changes in the absorption coefficient of the medium, by the tuning of the wavelength, or by changes in the light source–detector distance. The application for the *in vivo* monitoring of hemoglobin and oxyhemoglobin concentrations in human tissue is discussed. © 1997 Optical Society of America

Key words: Absorption coefficient, scattering coefficient, diffusion theory, intensity-modulated optical spectrometer.

1. Introduction

The analysis of absorption and scattering properties is an important problem in many areas of biomedical optics, in particular for determining hemoglobin (Hb), oxyhemoglobin (HbO_2), and cytochrome oxidase concentrations in tissue. Conventional near-infrared (NIR) spectroscopic methods allow the changes of chromophore concentrations to be calculated from changes in the light intensity diffusely reflected from the tissue surface.[1] However, the absolute concentrations of these chromophores, i.e., the absolute absorption coefficient, cannot easily be inferred, as the scattering of the light in the tissue has to be taken into account.

Different experimental approaches have been developed for the measurement of (absolute) absorption coefficients (μ_a) in highly scattering media, and these can be subdivided into two groups. The first group is based on intensity (reflectance) measurements for different distances between the light source and the detector. Farrell *et al.*[2] have shown that for multiple small source–detector distances, the reflectance measurements are sufficient to derive both the absorption and the transport scattering coefficients (μ_a and μ_s', respectively). Liu *et al.*[3] present an approximation for μ_a and μ_s' based on measurements of reflectance for multiple large source–detector distances. Similarly, when an estimated μ_s' is known, the absorption coefficient can be inferred from the slope of a plot of reflectance against distance.[4]

The second group is based on the measurement of the time of flight of the light in tissue in addition to the reflectance. Intensity-modulated optical spectrometers (IMOS's), which are an alternative to time-resolved systems, provide measurements of the phase and the modulation depth of an intensity-modulated lightwave. The phase difference is approximately proportional to the mean time of flight of the light in the medium. It has been shown that, for a fixed modulation frequency, μ_a and μ_s' can be inferred from the intensity and phase data obtained at different source–detector distances.[5–10] Alternatively, single-distance, multiple modulation frequency measurements can be used.[11–13] All these methods are based on the fitting of μ_a and μ_s' to diffusion equation solutions for light transport in the medium.

Here, a different approach for the determination of absorption coefficients is suggested. The basic finding is that small changes in the absorption coefficient induce changes in diffuse (reflected or transmitted) light intensity, time of flight (or phase), and modulation depth, and that the ratio of these changes is

primarily independent of the scattering properties of the medium. This ratio provides a good estimate of the absolute absorption coefficient. The approximation is valid over only a certain range of μ_a and μ_s' values; however, it encompasses the range found in biological tissues for NIR wavelengths. Similarly, the ratio of the changes in intensity and phase, induced by variations in the source–detector distance, allows μ_a to be estimated. Furthermore, μ_s' can be inferred based on the estimated μ_a value.

With this paper we aim to expand on the findings presented in a shorter publication.[14] In this paper the method is formulated in diffusion theory (Section 2) and used to determine the absorption coefficients of light-scattering, tissue-simulating phantoms (Section 3). In these experiments, changes in the absorption coefficient are induced by changes in chromophore concentrations. Alternatively, it is demonstrated that tuning the wavelength over the absorption spectrum of the chromophore allows the absorption coefficient (the mean μ_a over the tuned wavelength range) to be deduced. In addition, small changes in the source–detector distance are also exploited to obtain estimates of μ_a.

The main advantage of the suggested method for the *in vivo* monitoring of Hb concentration and oxygen saturation is its simplicity: a single light source and a single detector are sufficient, and the data evaluation is straightforward.

2. Description of the Method by Diffusion Theory

The transport of light in scattering media has been thoroughly analyzed over recent years, and diffusion theory has become established as a versatile tool for describing light intensity, time of flight, phase, and modulation depth in terms of the transport scattering coefficient (μ_s'), the absorption coefficient (μ_a), and the refractive index of the medium (n).[7,10,12,15–17]

For a pencil-beam light source on a semi-infinite half-space, the reflectance R (i.e., the number of photons backscattered to the surface of the medium per unit area) and the mean transit time (time of flight) $\langle t \rangle$ detected at a distance r from the source can be written as

$$R(r) = z_0\left(\frac{1}{\rho} + \mu_{\text{eff}}\right)\frac{\exp(-\mu_{\text{eff}}\rho)}{2\pi\rho^2}, \qquad (1)$$

$$\langle t \rangle(r) = \frac{\rho^2}{2c[D + \rho \cdot (\mu_a D)^{1/2}]}, \qquad (2)$$

respectively.[15,16] Here it is assumed that the pencil beam creates an isotropic photon source at depth z_0. In Eqs. (1) and (2), $\rho = (r^2 + z_0^2)^{1/2}$ and $z_0 = 1/\mu_s'$. The velocity of light in the medium $c = c_0/n$ (where the speed of light in vacuum is c_0). $\mu_{\text{eff}} = [3\mu_a(\mu_a + \mu_s')]^{1/2}$ is known as the effective attenuation coefficient, and $D = [3(\mu_a + \mu_s')]^{-1}$ is the diffusion coefficient.

When an IMOS is employed to measure chromophore concentrations, the phase Φ of a light-wave, intensity modulated at the frequency ν_M, is measured rather than the mean time. Φ and $\langle t \rangle$ are approximately coupled by the simple linear relationship[11,16]

$$\Phi = -2\pi\nu_M\langle t \rangle. \qquad (3)$$

This approximation is valid for the range of n, μ_a, and μ_s' values typical for tissue at NIR wavelengths and frequencies $\nu_M < 200$ MHz. Note that the phase Φ defined in Eq. (3) is negative with respect to $\langle t \rangle$.

Analytical expressions for the phase Φ and the modulation depth M (i.e., the ratio of the ac to the dc component of the modulated lightwave) can be derived. Patterson *et al.*[15] and Arridge *et al.*[16] obtained equations for Φ and M by performing a Fourier transformation of the temporally resolved impulse response of the reflectance $R(r, t)$. Patterson *et al.*[15] give the following equations:

$$\Phi = \Psi_r - \tan^{-1}\left(\frac{\Psi_r}{1 + \Psi_i}\right), \qquad (4)$$

$$M = \frac{(1 + \Psi_0^2 + 2\Psi_i)^{1/2}}{1 + \Psi_\infty}\exp(\Psi_\infty - \Psi_i), \qquad (5)$$

where $\Psi_0 = \mu_{\text{eff}}\rho(1 + \chi^2)^{1/4}$, $\Psi_r = -\Psi_0\sin(\theta/2)$, $\Psi_i = \Psi_0\cos(\theta/2)$, $\theta = \tan^{-1}(\chi)$, $\Psi_\infty = \mu_{\text{eff}}\rho$, and $\chi = (2\pi\nu_M)/(\mu_a c)$.

The linear relationship between $\langle t \rangle$ and Φ of Eq. (3) is valid for a near-symmetrical impulse response $R(r, t)$. For low μ_a (<0.005 mm^{-1}, which is at the lower end of the values typical for biological tissue), however, this is not fulfilled and, consequently, the values for Φ calculated from Eqs. (2) and (3) are different from those from Eq. (4) (for ν_M of the order of 100 MHz).

Equations (1)–(5) assume a matched boundary condition and do not take into account refractive-index differences between the medium and the surrounding that cause specular reflections at the boundary. All the conclusions drawn in this paper are equally valid when the mismatched boundary conditions[6,18] are included. To keep the equations as simple as possible, the matched boundary condition was used in preference to the mismatched boundary condition.

In the two subsections below, the changes in A, $\langle t \rangle$, Φ, and M with respect to variations in absorption coefficient and source–detector distance are examined.

A. Determination of μ_a: Changes in A, $\langle t \rangle$, Φ, and M with Respect to μ_a

Here the changes in reflectance, mean time, phase, and modulation depth are examined with respect to pure μ_a changes. The derivative of attenuation A [defined as the logarithm (base 10) of the ratio of

incident and detected intensities] and $\langle t \rangle$ with respect to changes in μ_a can be derived from Eqs. (1) and (2), giving

$$\frac{\partial A}{\partial \mu_a} = \frac{3}{2 \ln 10} \frac{\rho}{1/\rho + \mu_{\text{eff}}} (2\mu_a + \mu_s'), \qquad (6)$$

$$\frac{\partial \langle t \rangle}{\partial \mu_a} = \frac{-3}{2(1/\rho + \mu_{\text{eff}})^2 c} \left[\frac{\rho}{2} \frac{\mu_s'}{(\mu_a D)^{1/2}} - 1 \right]. \qquad (7)$$

We are interested in the quotient $Q_a = (\partial A/\partial \mu_a)/(\partial \Phi/\partial \mu_a)$ of these two quantities. This ratio can be simplified by the use of the diffusion approximation, which states that scattering dominates absorption ($\mu_a \ll \mu_s'$), and therefore $\mu_{\text{eff}} \cong (3\mu_a \mu_s')^{1/2}$ and $D \cong (3\mu_s')^{-1}$. When these approximations are used, the ratio of Eqs. (6) and (7) becomes

$$\left(\frac{\partial A}{\partial \mu_a} \right) \bigg/ \left(\frac{\partial \langle t \rangle}{\partial \mu_a} \right) = \frac{-(1 + \rho\mu_{\text{eff}})c}{\ln 10 \left(\frac{\rho\mu_{\text{eff}}}{2} - \frac{\mu_a}{\mu_s'} \right)} \mu_a. \qquad (8)$$

For media with optical properties similar to tissue ($\mu_s' = 1$–2 mm^{-1}; $\mu_a = 0.005$–0.05 mm^{-1}) and typical source–detector distances ($r = 20$–40 mm), $\rho\mu_{\text{eff}}/2 \gg \mu_a/\mu_s'$, and therefore

$$\left(\frac{\partial A}{\partial \mu_a} \right) \bigg/ \left(\frac{\partial \langle t \rangle}{\partial \mu_a} \right) = \frac{-2(1/\mu_{\text{eff}} + \rho)c}{\ln 10 \rho} \mu_a. \qquad (9)$$

Furthermore, for large source–detector distances ($\rho \gg 1/\mu_{\text{eff}}$), Eq. (9) is, to a good approximation, independent of both μ_s' and ρ. Equation (9) can therefore be reduced to

$$\left(\frac{\partial A}{\partial \mu_a} \right) \bigg/ \left(\frac{\partial \langle t \rangle}{\partial \mu_a} \right) k = \frac{-2c}{\ln 10} \mu_a, \qquad (10)$$

which is a linear function of μ_a (and c) only.

Figure 1(a) shows the quotient $Q_a = (\partial A/\partial \mu_a)/(\partial \Phi/\partial \mu_a)$. The solid lines are the exact solutions calculated from Eqs. (3), (6), and (7) for transport scattering coefficients of $\mu_s' = 1.0$, 1.25, and 1.5 mm^{-1}, a source–detector distance of $r = 30$ mm, a modulation frequency of $\nu_M = 200$ MHz, and a refractive index of $n = 1.33$. To a good approximation, Q_a varies linearly with μ_a. The approximations for Q_a given by Eqs. (9) and (10) [dashed and dotted lines in Fig. 1(a), respectively, calculated for $\mu_s' = 1.5$ mm^{-1}] are also shown. Although Eq. (10) produces a 15% underestimate compared with the exact solution for Q_a, Eq. (9) is a reasonable approximation of the Q_a versus μ_a relationship.

It is remarkable that Q_a is dependent primarily on μ_a only, with a variation in μ_s' from 1 to 1.5 mm^{-1}, having only a small influence on Q_a. Consequently a good estimate of the absolute (mean) absorption coefficient can be obtained by the measurement of the ratio of attenuation and phase changes for variations in the absorption coefficient.

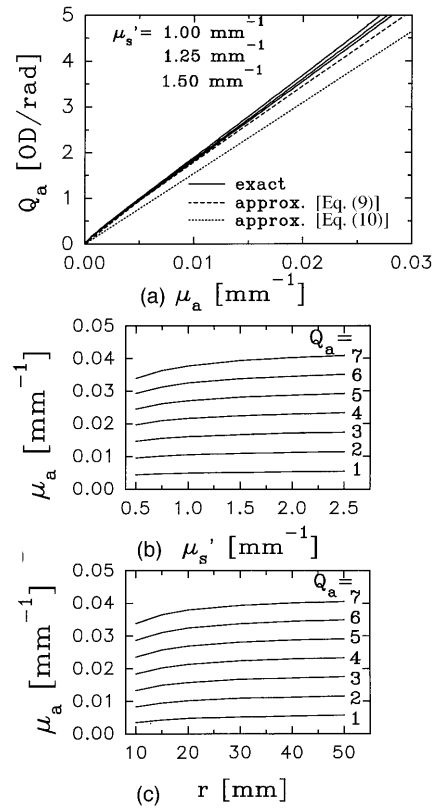For any experimentally determined value of Q_a it is crucial to estimate the influence of μ_s' and r (source–

Fig. 1. (a) $Q_a = (\partial A/\partial \mu_a)/(\partial \Phi/\partial \mu_a)$ as a function of μ_a for $\nu_M = 200$ MHz, $n = 1.33$, and a source–detector distance of $r = 30$ mm. The solid lines represent Q_a calculated from Eqs. (3), (6), and (7) for values of $\mu_s' = 1.0$, 1.25, and 1.5 mm^{-1}. The dashed and the dotted lines are the approximations of Eqs. (9) and (10), respectively, calculated for $\mu_s' = 1.5$ mm^{-1}. (b) Curves of constant Q_a [in units of optical density per radian (OD/rad)] as a function of μ_s' and μ_a calculated for $\nu_M = 200$ MHz, $n = 1.33$, and $r = 30$ mm. (c) Curves of constant Q_a [in units of optical density per radian (OD/rad)] as a function of r and μ_a calculated for $\mu_s' = 1.5$ mm^{-1} ($\nu_M = 200$ MHz, $n = 1.33$).

detector spacing) on the estimate of μ_a. Curves of constant Q_a are shown in Fig. 1(b) as a function of μ_a and μ_s'. Figure 1(b) demonstrates that changing the assumed value for μ_s' from 0.5 to 2.5 mm^{-1} (i.e., a range in μ_s' that is much larger than would be expected for a specific tissue type), at a source–detector distance of 35 mm, gives corresponding absorption coefficients that vary by less than 20%. This variation in μ_a is approximately the same for the range in Q_a considered here. The curves in Fig. 1(b) suggest that the influence of μ_s' on the estimate of μ_a decreases with increasing μ_s'.

Furthermore, any experiment is prone to slight uncertainties in the source–detector distance. The variation in μ_a derived from constant values of Q_a as a function of r is shown in Fig. 1(c). The curves in Fig. 1(c) demonstrate that an estimate of μ_a is relatively insensitive to uncertainties in the source–detector distance of 5 mm.

The derivatives of phase Φ and modulation depth M with respect to μ_a can be derived from Eqs. (4) and
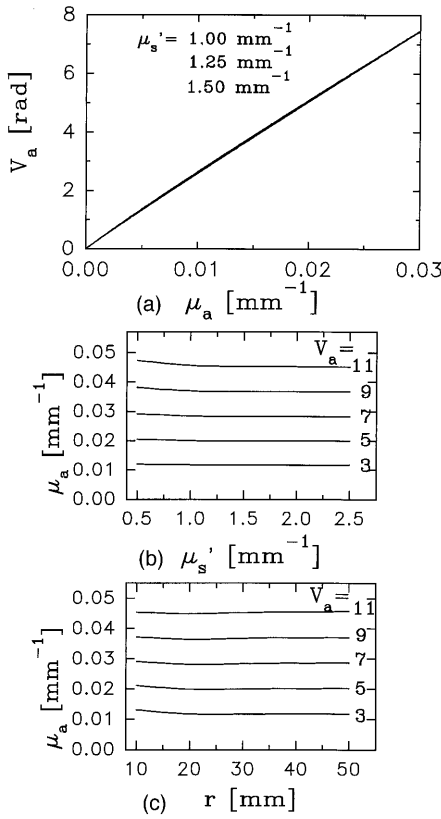
Fig. 2. (a) $V_a = (\partial\Phi/\partial\mu_a)/(\partial M/\partial\mu_a M^{-1})$ calculated for the same optical properties as in Fig. 1(a), (b) curves of constant V_a as a function of μ_s' and μ_a for $r = 30$ mm, (c) curves of constant V_a as a function of r and μ_a calculated for $\mu_s' = 1.5$ mm^{-1}. ($\nu_M = 200$ MHz, $n = 1.33$).

(5), giving

$$\frac{\partial\Phi}{\partial\mu_a} = \frac{1}{1 + \Psi_0^2 + 2\Psi_i}\left[\frac{\partial\Psi_0}{\partial\mu_a}\Psi_0(\Psi_r - \sin\theta)\right.$$
$$\left. - \frac{\partial\theta}{\partial\mu_a}\frac{\Psi_0^2}{2}(\Psi_i + \cos\theta)\right], \qquad (11)$$

$$\frac{\partial M}{\partial\mu_a} = \frac{M}{1 + \Psi_0^2 + 2\Psi_i}\left[-\frac{\partial\theta}{\partial\mu_a}\frac{\Psi_0^2}{2}(\Psi_r - \sin\theta)\right.$$
$$\left. - \frac{\partial\Psi_0}{\partial\mu_a}\Psi_0(\Psi_i + \cos\theta)\right] + \frac{3M(2\mu_a + \mu_s')\rho^2}{2(1 + \Psi_\infty)}, \qquad (12)$$

where

$$\frac{\partial\Psi_0}{\partial\mu_a} = \frac{3\rho^2}{2\Psi_0(1 + \chi^2)^{1/2}}[\mu_a(2 + \chi^2) + \mu_s'],$$

$$\frac{\partial\theta}{\partial\mu_a} = \frac{-\chi}{(1 + \chi^2)\mu_a}.$$

The quotient $V_a = (\partial\Phi/\partial\mu_a)/(\partial M/\partial\mu_a M^{-1})$ derived from Eqs. (11) and (12) is plotted in Fig. 2(a) for the same optical coefficients used to derive Q_a in Fig. 1(a). Like Q_a, V_a is, to a good approximation, a linear

function of μ_a. Figures 2(b) and 2(c) show that the influence of μ_s' on V_a is even smaller than its influence on Q_a. For a V_a of 7 rad, a variation of μ_s' between 0.5 and 2.0 mm^{-1} or a variation of r between 20 and 50 mm changes the corresponding values of μ_a by <2%. Consequently, measuring V_a gives a more precise estimate of μ_a than measuring Q_a.

B. Determination of μ_a: Change in A, $\langle t \rangle$, Φ, and M with Respect to r

A number of papers have examined using variations of measurements from IMOS's as a function of distance to determine optical properties.[7–10] They have concentrated on using the measurements $\log(rR)$, $\log(rRM)$, and Φ, i.e., the product of source–detector distance and dc intensity, the product of source–detector distance and the ac intensity, and phase measurements. Modulation depth measurements have been briefly discussed but largely discounted as producing inferior solutions to optical properties. Here we remove the source–detector distance term to examine how important it is to know this parameter accurately, and we also examine further the use of modulation depth measurements.

The derivatives of attenuation, mean time, phase, and modulation depth with respect to the source–detector distance r derived from Eqs. (1), (2), (4), and (5) are

$$\frac{\partial A}{\partial r} = \frac{1}{\rho^2(1/\rho + \mu_{\text{eff}})} + \frac{1}{\ln 10}(2/\rho + \mu_{\text{eff}}), \qquad (13)$$

$$\frac{\partial\langle t \rangle}{\partial r} = \frac{3(2/\rho + \mu_{\text{eff}})}{2c(1/\rho + \mu_{\text{eff}})^2}(\mu_s' + \mu_a), \qquad (14)$$

$$\frac{\partial\Phi}{\partial r} = \frac{r}{\rho^2}\Psi_r\left(\frac{\Psi_0^2 + 2\Psi_i}{1 + \Psi_0^2 + 2\Psi_i}\right), \qquad (15)$$

$$\frac{\partial M}{\partial r} = \frac{r}{\rho^2}M\left[\frac{\Psi_0^2 - (\Psi_0^2 + 2\Psi_i)\Psi_i}{1 + \Psi_0^2 + 2\Psi_i} + \frac{\Psi_\infty^2}{1 + \Psi_\infty}\right]. \qquad (16)$$

The quotients $Q_r = (\partial A/\partial r)/(\partial\Phi/\partial r)$ calculated from Eqs. (3), (13), and (14) and $V_r = (\partial\Phi/\partial r)/(\partial M/\partial r M^{-1})$ derived from Eqs. (15) and (16) are shown in Figs. 3(a) and 4(a), respectively, as a function of μ_a. To allow comparison with the experimental data presented in Subsection 3.B.3., a refractive index of $n = 1.56$ and a source–detector distance of $r = 35$ mm were assumed. Q_r is negative as attenuation and mean time increase with distance while the phase decreases [see Eq. (3)].

The dependence of Q_r and V_r on μ_a is similar to that of Q_a and V_a. The magnitude of both functions increases approximately linearly with μ_a and the influence of μ_s' and r is small. The errors in the μ_a estimate that arise from uncertainties in μ_s' and r are of the same order for both Q_r and Q_a (compare Figs. 3 and 1). When Q_r is used, variations in μ_s' between 0.5 and 2.5 mm^{-1} and source–detector separations of 25 to 50 mm result in derived μ_a values that vary by up to 25% at $\mu_a = 0.01$ mm^{-1}, less at higher μ_a.
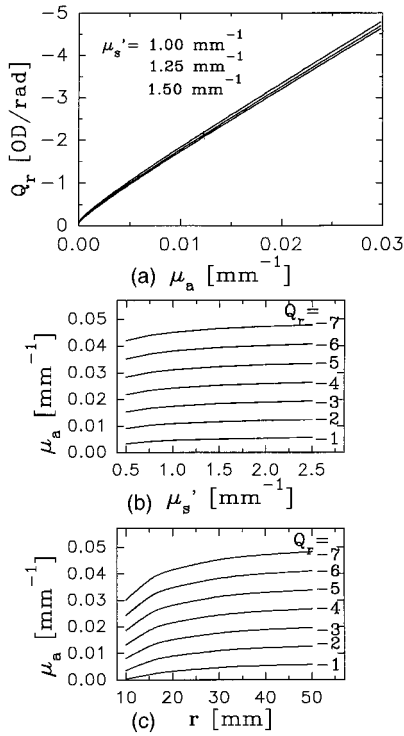
Fig. 3. (a) $Q_r = (\partial A/\partial r)/(\partial \Phi/\partial r)$ as a function of μ_a calculated from Eqs. (3), (13), and (14) for $r = 35$ mm, $n = 1.56$ and $\mu_s' = 1.0$, 1.25, and 1.50 mm^{-1}; (b) curves of constant Q_r as a function of μ_s' and μ_a calculated for $r = 30$ mm; (c) curves of constant Q_r as a function of r and μ_a calculated for $\mu_s' = 1.5$ mm^{-1} ($\nu_M = 200$ MHz, $n = 1.56$).

When V_r is used (see Fig. 4), the same variations in μ_s' and r result in uncertainties in μ_a of less than 4%. Consequently the same conclusion can be drawn for Q_r and V_r as for Q_a and V_a: measuring changes in A and Φ or Φ and M for varying source–detector distances allows μ_a to be estimated from $Q_r = \Delta A/\Delta \Phi$ or $V_r = \Delta \Phi/\delta M$ ($\delta M = \Delta M/M$) .

C. Determination of μ_s'

Subsections 2.A and 2.B describe how the absorption coefficient can be estimated from quotients Q_a, V_a, Q_r, or V_r. Once an estimate of μ_a is obtained, the equations for R, Φ, and M are dependent on only one variable: μ_s' (assuming that n is known). Therefore various techniques can be used to derive μ_s'. For example, μ_s' can be acquired from measurements of the absolute phase by the solution of Eqs. (2) and (3) or Eq. (4). Alternatively, the attenuation, phase, or modulation depth differences measured for at least two source–detector distances can be exploited by the solution of the equation for either ΔA, $\Delta \Phi$, or ΔM and μ_s'. A prerequisite is that the exact magnitude of the change in r is known.

For example, assume that $\Delta A = \log[R(r_1)/R(r_2)]$ and $\Delta \Phi = \Phi(r_2) - \Phi(r_1)$ have been measured at the distances r_1 and $r_2 = r_1 + \Delta r$ (where $\Delta r \ll r_1$). $\Delta A/\Delta \Phi$ gives an estimate of μ_a according to Subsection 2.B. With this estimated μ_a, μ_s' can be calculated from ΔA by Eq. (1). For $r_1 \gg 1/\mu_{\text{eff}}$, the
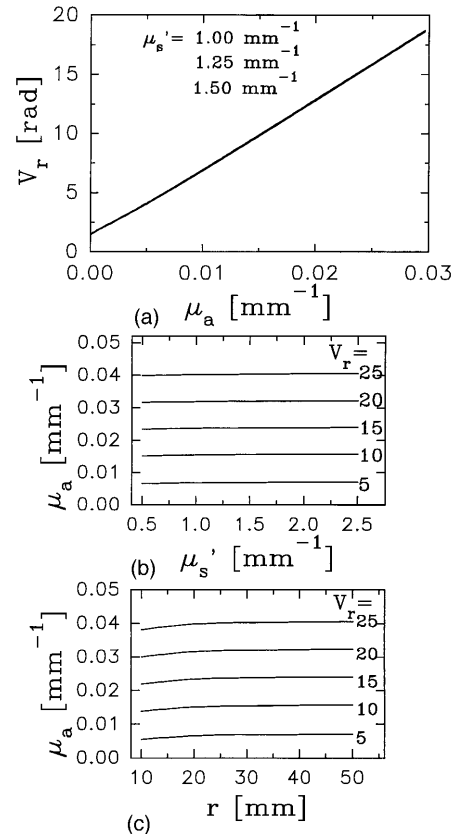

Fig. 4. (a) $V_r = (\partial \Phi/\partial r)/(\partial M/\partial r M^{-1})$ calculated from Eqs. (15) and (16) for the same optical properties as in Fig. 3, (b) curves of constant V_r as a function of μ_s' and μ_a calculated for $r = 30$ mm, (c) curves of constant V_r as a function of r and μ_a calculated for $\mu_s' = 1.5$ mm^{-1} ($\nu_M = 200$ MHz, $n = 1.56$).

approximation

$$\mu_s' = \left\{ \left[\Delta A - \log\left(\frac{r_2^2}{r_1^2}\right) \right] \frac{\ln 10}{\Delta r} \right\}^2 \frac{1}{3\mu_a} \quad (17)$$

is valid.

In this approximation, μ_s' has the same systematic error as μ_a. In a similar manner, $\Delta \Phi$ or ΔM can be used for a calculation of μ_s'.

3. **Experimental Determination of Absorption Coefficients**

A. Method

1. *Intensity-Modulated Optical Spectrometer*
The IMOS used for all the experiments discussed in this paper has been described in detail previously.[11] It incorporates four different laser diodes ($\lambda = 744$, 807, 832, 860 nm) that are intensity modulated at a frequency of $\nu_M < 500$ MHz. Phase-sensitive (lock-in) amplifiers allow phase shifts and changes in the modulation depth of multiply scattered light to be detected. Optical fibers were used to transport the light between the diode lasers, the scattering media, and the photomultipier detector. The wavelength of a fifth diode laser could be varied between 753 and

Table 1. Optical Properties of the Liquid-Scattering Phantom used for Four Different Wavelengths λ[a]

λ (nm)	μ_s' (mm^{-1})	$\mu_a = \mu_a^d + \mu_a^w$ (mm^{-1})	$\Delta A/\Delta \Phi$ (OD/rad)	μ_a (mm^{-1}) (± 0.0008)
	Phantom Properties		Experimental	
744	1.22	0.0133	2.47	0.0135
807	1.18	0.0142	2.66	0.0144
832	1.16	0.0157	2.93	0.0158
860	1.13	0.0169	3.08	0.0166

[a]The values for μ_s' were derived from Mie theory. μ_a (third column) consists of the dye absorption μ_a^d and the water absorption μ_a^w. The last two columns give the measured ratio of the attenuation and phase change ($Q_a = \Delta A/\Delta \Phi$) and the corresponding absorption coefficient (μ_a) derived from Eqs. 1–3 (compare with Fig. 1 and 8). These estimates are based on variations in μ_s' between 0.75 and 2.0 mm^{-1}, resulting in uncertainties of $\Delta\mu_a = \pm 0.0008$ mm^{-1}.

761 nm by a change in its temperature. The linewidth of this laser was 2 nm (full width at half-maximum).

The IMOS measures changes in attenuation [A, in units of optical density (OD)], phase (Φ, in units of radians), and modulation depth (M, the ratio of the ac and the dc amplitudes, i.e., it is unitless). Although phase differences $\Delta\Phi = \Phi_2 - \Phi_1$ (in radians) can be measured without correction for the characteristics of the IMOS, absolute changes in the modulation depth $\Delta M = M_2 - M_1$ require a reference measurement. However, the fractional change $\delta M = \Delta M/M$ can be obtained without calibration. (Throughout this paper Δ always symbolizes an absolute change, whereas δ describes a fractional change.)

2. Scattering Phantoms

Two different light-scattering, tissue-simulating phantoms of known absorption and transport scattering coefficients were employed to demonstrate the feasibility of the suggested method.

The first phantom consisted of spherical polystyrene particles (B. Harness, Department of Chemical Engineering, University of Bradford, U.K.) that served as light-scattering centers. The spheres were suspended in water. Mie theory[19] was used to derive the scattering cross section and transport scattering coefficient μ_s' of these spheres (diameters between 0.6 and 2.5 μm). The calculated scattering cross section was found to be in agreement with attenuation measurements performed in a collimated beam setup.[20] For a sphere concentration of $c_s = 1\%$ volume/volume (v/v), the calculated μ_s' was approximately 1.2 mm^{-1} (see Table 1). The absorption coefficient of the phantom μ_a was the sum of the water absorption (μ_a^w) and the absorption (μ_a^d) of a dye (S109564, ICI, Manchester, U.K.) that was added in known quantities to the water: $\mu_a = \mu_a^w + \mu_a^d$. The spectra of μ_a^w, μ_a^d, and $\mu_a^w + \mu_a^d$ are shown in Fig. 5 for a dye concentration of $c_d = 1.40 \times 10^{-5}$ v/v. The tips of the light delivery and detection fibers of
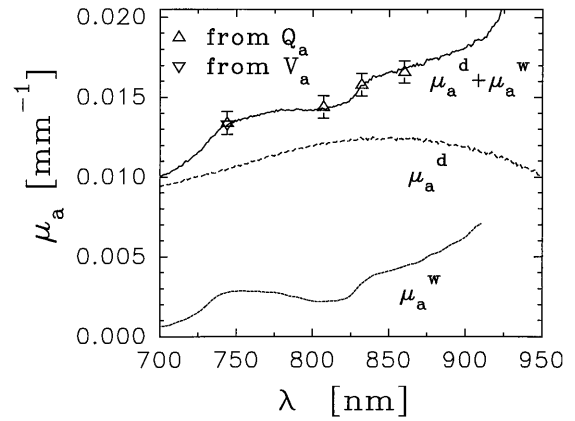

Fig. 5. Absorption coefficient $\mu_a = \mu_a^w + \mu_a^d$ of the liquid phantom, where μ_a^w is the water absorption and μ_a^d is the dye absorption for a concentration of $c_d = 1.40 \times 10^{-5}$ v/v. The dots are the absorption coefficients for the four laser wavelengths (see Fig. 7) derived experimentally from $Q_a = \Delta A/\Delta \Phi$ and $V_a = \Delta\Phi/\delta M$ (for 744 nm) and based on μ_s' values between 0.75 and 2.0 mm^{-1}.

the IMOS were submerged approximately 2 mm into the phantom (volume 100 mm × 80 mm × 60 mm).

The second, solid phantom was made of epoxy resin (see Firbank et al.[21]). An absorbing dye (Pro Jet 900NP, Zeneca Ltd, Manchester, U.K.) was added to the resin (refractive index 1.56). The light-scattering centers were amorphous silica spheres of 1.0-μm diameter with a methacrylate coating (Monospher 1000M, E. Merck, Darmstadt, Germany) and they were suspended in the resin. The wavelength dependence of μ_a and μ_s' of this phantom is shown in Fig. 6. The fractional errors in μ_a and μ_s' are approximately $\pm 2\%$. The ends of the optical fibers were positioned less than 1 mm above the phantom. The high refractive index of the epoxy resin results in a high degree of specular reflection at the boundary between the phantom and air. To reduce these specular reflections, the surface of the phantom around and between the fibers was covered with black tape with a refractive index higher than that of air.
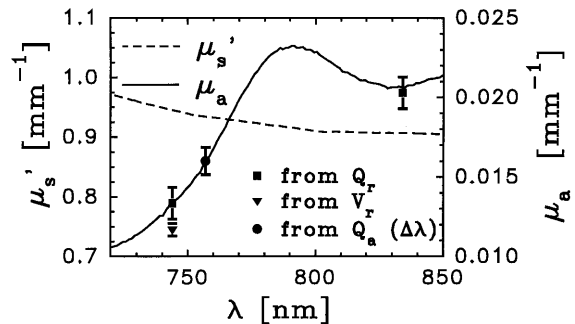

Fig. 6. Absorption coefficient μ_a (solid curve) and transport scattering coefficient μ_s' (dashed curve) of the solid phantom (errors approximately $\pm 2\%$). The absorption coefficients derived from $Q_a(\Delta\lambda)$ (filled circle; compare with Fig. 8), Q_r (filled squares, compare with Fig. 9), and V_r (filled triangle, for 744 nm) are shown. The error bars represent the variations in μ_a under the assumption that 0.75 mm$^{-1} < \mu_s' < 2$ mm^{-1}.
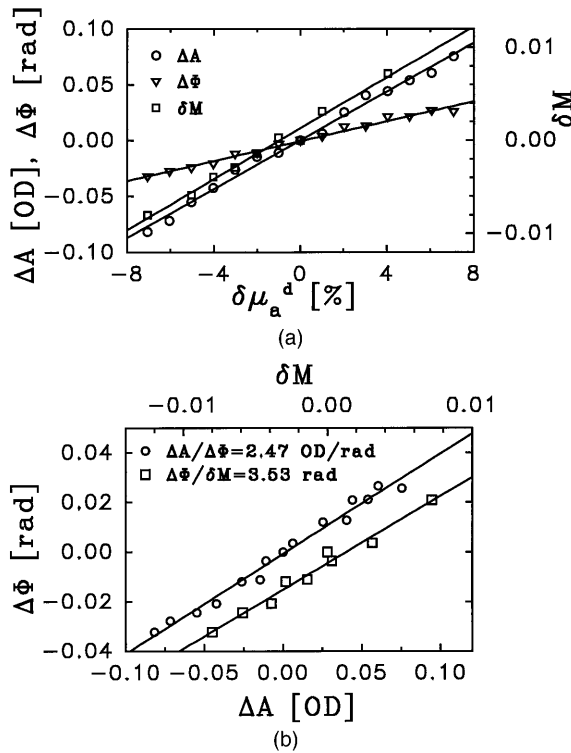
Fig. 7. (a) Measured changes in attenuation ΔA, phase $\Delta \Phi$, and modulation depth $\delta M = \Delta M/M$ as a function of changes in dye absorption $\delta \mu_a^d$ for $\lambda = 744$ nm. The lines give a first-order regression fit through the experimental data. (b) Correlation plots of both ΔA and δM with $\Delta \Phi$ for the data of (a). The regression lines have slopes of $Q_a = \Delta A/\Delta \Phi = 2.47$ OD/rad and $V_a = \Delta \Phi/\delta M = 3.53$ rad.

B. Determination of μ_a in Scattering Phantoms

1. Changes in Concentration c_d of Chromophores:
$Q_a(\Delta c_d)$ and $V_a(\Delta c_d)$

The absorption coefficient μ_a of the liquid, light-scattering phantom was changed when the concentration of the dye was varied in 14 steps of $\delta \mu_a^d = 1.44\%$ each (corresponding to $\Delta \mu_a = 1.56 \times 10^{-4}$ mm^{-1} at $\lambda = 744$ nm). The concentration of the light-scattering microspheres was $c_s = 1\%$ v/v and was held constant during the experiment. The resulting optical properties of the liquid phantom are listed in Table 1 for the four different laser wavelengths of the IMOS. The values of μ_a given in the table are for a dye concentration of $c_d = 1.40 \times 10^{-5}$ v/v. The wavelength dependence of μ_s' is insignificant, whereas μ_a varies by ~30% for the four laser wavelengths. The changes in attenuation, phase, and modulation depth were recorded with the IMOS as a function of the absorption changes $\delta \mu_a^d$. This is shown in Fig. 7(a) for $\lambda = 744$ nm. Plotting ΔA against $\Delta \Phi$ [see Fig. 7(b)] shows a strong correlation with a first-order regression slope $Q_a = \Delta A/\Delta \Phi = 2.47$ OD/rad. When this measured value of Q_a and the known transport scattering coefficient are used, Eqs. (3), (6), and (7) and Fig. 1 allow an absorption coefficient of $\mu_a = 0.0135$ mm^{-1} to be calculated.

This is in excellent agreement with the true value. The experimental values of Q_a and μ_a derived in the same manner for all four wavelengths are listed in the fourth and the fifth columns of Table 1 and are shown in the absorption spectrum of Fig. 5. The μ_a values given in the table are based on μ_s' between 0.75 and 2.0 mm^{-1}, which result in uncertainties of approximately ± 0.0008 mm^{-1}. All the μ_a values calculated in this manner agree with the true absorption coefficients to within the above uncertainties.

The correlation between $\Delta \Phi$ and $\delta M = \Delta M/M$ is included in Fig. 7(b) ($\lambda = 744$ nm). The first-order regression has a slope of $\Delta \Phi/\delta M = 3.53$ rad. Taking this slope as V_a and evaluating according to Eqs. (11) and (12) [compare with Fig. 2(a)] gives an estimate of $\mu_a = 0.0133$ mm^{-1} ($\pm 1\%$) for 0.75 mm$^{-1} < \mu_s' < 2.0$ mm^{-1}.

2. Changes in Wavelength λ: $Q_a(\Delta \lambda)$ and $V_a(\Delta \lambda)$

The second approach to obtain values of $\Delta A/\Delta \Phi$ or $\Delta \Phi/\delta M$ is to induce small changes in the absorption coefficient by the tuning of the wavelength λ, i.e., to scan over the absorption spectrum of the scattering medium. A prerequisite is that μ_s' remains unchanged over the range of wavelengths used or that changes in μ_s' can be accounted for.

The solid, light-scattering phantom with well-characterized optical properties (compare with Fig. 6 for $\lambda = 758$ nm: $\mu_a = 0.0160$ mm, $\mu_s' = 0.934$ mm, $n = 1.56$) had fractional changes in μ_a and μ_s' with wavelength of $\delta \mu_a \cong +1.5\%$/nm and $\delta \mu_s' \cong -0.05\%$/nm, i.e., the changes in μ_s' were much smaller than those in μ_a. The light reflected from the phantom was detected at a distance of $r = 30$ mm from the light source. Variations in the diode laser output with changing wavelength were corrected by reference measurements of intensity, phase, and modulation depth at a distance of $r = 7$ mm. Figure 8(a) shows the changes in A, Φ, and M as a function of wavelength relative to the values recorded at $\lambda = 758$ nm. A, Φ, and M increase with wavelength, which is consistent with an absorption coefficient's increasing (see Fig. 6).

The correlation of ΔA and $\Delta \Phi$ for this wavelength range [see Fig. 8(b)] has a first-order regression slope of $Q_a = 2.23$ OD/rad. By analysis of this value according to Eqs. (3)–(5), an absorption coefficient of $\mu_a = 0.0161$ (± 0.0008) mm^{-1} was calculated based on 0.75 mm$^{-1} < \mu_s' < 2.0$ mm^{-1}. The first-order regression slope of $\Delta \Phi/\delta M$ [Fig. 8(b)] has a correlation coefficient of $V_a = 5.03$ rad, which corresponds to a value of $\mu_a = 0.0168$ mm^{-1} ($\pm 1\%$) for the same range of μ_s'.

The μ_a values derived from $Q_a(\Delta \lambda)$ and $V_a(\Delta \lambda)$ are in excellent agreement with the true value.

3. Changes in Source–Detector Distance r:
Q_r and V_r

The changes in attenuation, phase, and modulation depth were measured as a function of the source–detector distance for the solid-scattering phantom. This is shown in Fig. 9(a) for $\lambda = 744$ nm. The
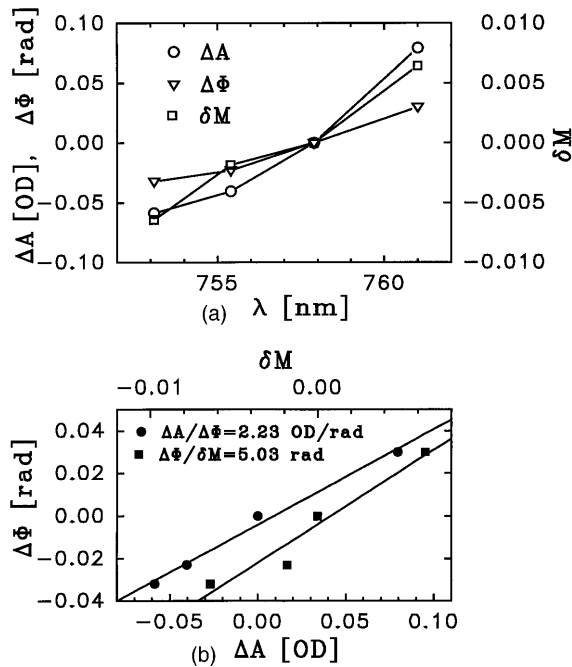
Fig. 8. (a) Changes in attenuation (ΔA), phase ($\Delta\Phi$), and modulation depth ($\delta M = \Delta M/M$) as a function of wavelength λ, (b) correlation of ΔA and δM with $\Delta\Phi$ for the data of (a). A first-order regression gives slopes of $Q_a = \Delta A/\Delta\Phi = 2.23$ OD/rad and $V_a = \Delta\Phi/\delta M = 5.03$ rad.
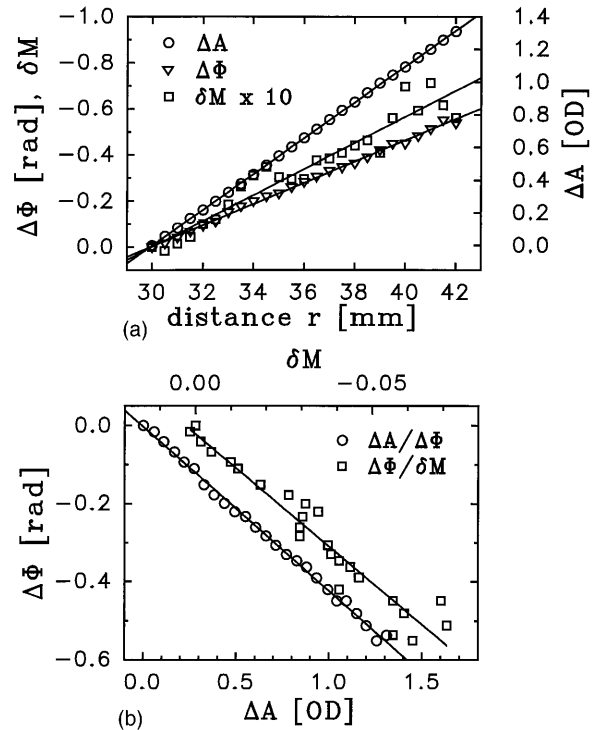

Fig. 9. (a) Changes in attenuation (ΔA), phase ($\Delta\Phi$), and modulation depth ($\delta M = \Delta M/M$) as a function of source–detector distance r, measured on a solid phantom ($\mu_a = 0.0135$ mm^{-1}, $\mu_s' = 0.94$ mm^{-1}, $n = 1.56$ for $\lambda = 744$ nm; compare with Fig. 6). The solid lines give the first-order regression through the data. Note that the scale for δM is expanded by a factor of 10. (b) Correlation of both ΔA and δM with $\Delta\Phi$ for the data shown in (a). The first-order regression lines have slopes of $Q_r = \Delta A/\Delta\Phi = 2.38$ OD/rad and $V_r = \Delta\Phi/\delta M = 7.6$ rad. The absorption coefficient μ_a derived from $Q_r = \Delta A/\Delta\Phi$ is shown in Fig. 6.

first-order regression of these experimental data has slopes of $\Delta A/\Delta r = 0.11$ OD/mm, $\Delta\Phi/\Delta r = -0.046$ rad/mm, and $\delta M/\Delta r = \Delta M/M = -0.00575$/mm. This agrees well with the theoretical slopes ($\Delta A/\Delta r = 0.1105$ OD/mm, $\Delta\Phi/\Delta r = -0.0457$ rad/mm, and $\delta M/\Delta r = -0.00522$/mm) calculated with the known properties of the phantom ($\mu_a = 0.0135$ mm^{-1}, $\mu_s' = 0.94$ mm^{-1}, $n = 1.56$ for $\lambda = 744$ nm; see Fig. 6) and Eqs. (1)–(5). In Fig. 9(b), the correlation of both ΔA and δM with $\Delta\Phi$ is shown ($\lambda = 744$ nm). The first-order regression of ΔA and $\Delta\Phi$ has a slope of $Q_r = \Delta A/\Delta\Phi = 2.38$ OD/rad. On the use of Eqs. (13) and (14) [compare Figs. 3(a) and 3(b)] and assuming transport scattering coefficients between 0.75 mm$^{-1} < \mu_s' < 2$ mm^{-1}, an absorption coefficient of $\mu_a = 0.0137$ (± 0.0010) mm^{-1} was obtained. This value is shown in Fig. 6 together with the absorption coefficients derived in an equivalent manner for $\lambda = 832$ nm. For the other two wavelengths of the IMOS, the received light intensity was too low to derive $\Delta A/\Delta\Phi$. Analyzing the measured ratio $V_r = \Delta\Phi/\delta M = 0.0565$ rad [Fig. 9(b)] gives $\mu_a = 0.0117$ mm^{-1} (± 0.0001 mm^{-1}) for the same range of μ_s' [compare with Fig. 3(a)].

Using the estimated value of μ_a together with the measured attenuation change ΔA/mm allows the transport scattering coefficient to be calculated from Eq. 1. The measured slope $\Delta A/\Delta r = 0.11$ OD/mm ($\lambda = 744$ nm) gives $\mu_s' = 0.900$ (± 0.065) mm^{-1} for $\mu_a = 0.0135$ (± 0.001) mm^{-1}. Evaluating this slope according to the approximation of Eq. (11) provides a value for μ_s' of 0.95 (± 0.065) mm^{-1}. In a similar

way, the slope of the phase can be used. For $\Delta\Phi/\Delta r = -0.046$ rad/mm and the estimated μ_a, Eq. (2) gives a transport scattering coefficient of $\mu_s' = 0.902$ (± 0.065) mm^{-1}. These values are in agreement with the true μ_s'.

4. Discussion and Conclusion

The method described here allows the absolute absorption coefficient (chromophore concentration) in highly scattering media to be determined from the quotient of changes in either attenuation and phase (Q quotient) or phase and modulation depth (V quotient). The diffusion equation modeling in Section 2 showed that either the quotient Q or V could be used where modifications to measurements were made either by small changes to the medium's μ_a or r (source–detector spacing). The use of small changes in μ_a of unknown magnitude to obtain absolute values for μ_a is a new discovery to our knowledge. The use of changes in distance has been investigated before[8–10]; however, here we suggest that knowledge of the source–detector distance at which measurements are made is not a requirement of such a measurement strategy.

A consideration in using IMOS technology is the choice of modulation frequency. In the modeling

here it has been such that $\omega \ll \mu_a c$ and, although this is not essential, it is advantageous. The relationships in Figs. 1–4 become more complex and potentially ambiguous if $\omega \gg \mu_a c$ (for human tissues at NIR wavelengths of $\omega = \mu_a c$ near 400 MHz).

The modeling assumes matched boundary conditions, which was satisfactory judging by the excellent agreement between μ_a determined with the V and Q quotients and true μ_a. Fantini et al.[8] suggest that boundary conditions do affect the slopes of dc intensity and phase with distance by 5% to 10%; these variations may well cancel out to some extent in the quotients.

The accuracy of μ_a determined with the V and Q quotients is good, as judged by the comparison against true μ_a in Figs. 5 and 6. The error bars in these figures, in which the Q quotient is used, represent a theoretical uncertainty, assuming that μ_s' is unknown but lies in the range 0.75–2 mm^{-1}. The theoretical error bars for the V quotient would have been approximately a factor of 5 smaller.

Figures 5 and 6 do not show the Q and V quotient data for all four wavelengths of the IMOS system, as low light intensities prevented the collection of data with sufficient signal-to-noise ratio at some wavelengths. Although the diffusion equation modeling suggests that the V quotient is the best to use as it is less sensitive to source–detector separation and scattering coefficient, it has the disadvantage that the noise on the measured V quotient is some 5 to 10 times larger than the Q quotient for the same detected light intensity and measurement interval. Hence, to make use of the inherent greater insensitivity of the V quotient to r and μ_s', either a significantly larger measurement time or light intensity is required.

The experiments performed on tissue-simulating phantoms discussed in Section 4 demonstrate three different approaches that can be used to induce the μ_a and r changes. It is possible that all three could be useful for monitoring Hb and HbO$_2$ in vivo.

(1) The first option is to use small variations in the absorption coefficient. In the experiment described in Subsection 3.B.1 this was achieved when dye was added to a liquid phantom. The absolute magnitude of the change in the chromophore concentration is not required. In many in vivo situations it is therefore sufficient to rely on changes in chromophore concentrations that occur spontaneously, i.e., those that occur through changes in blood volume or blood oxygenation. For example, one possible application is the monitoring of blood volume and oxygen saturation in the brain of fetuses. During labor, contractions increase the pressure on the fetus and therefore induce shifts in the blood volume and changes in the blood supply. This is especially true for the fetal head, and, as a consequence, hypoxic states of the brain can occur that could lead to neurological impairments. The first promising experiments to monitor these changes in Hb and HbO$_2$ in vivo have been performed with the IMOS system, and absolute absorption coefficients and oxygen saturations were calculated.[22] However, as no other reliable method for monitoring the Hb–HbO$_2$ status in the brain exists, a validation of the values obtained was not possible.

(2) In the second experiment (see Subsection 3.B.2), changes in A, Φ, and M were induced by the tuning of the wavelength of a diode laser over the absorption spectrum of a chromophore. Alternatively, different laser light sources with closely adjacent wavelengths or a white-light source in combination with a wavelength-selective element could be used. It is not necessary to know the absolute shift in wavelength to estimate μ_a. In all practical applications, this method is clearly limited by the possibility that it may not be feasible to neglect the effect of scattering changes with wavelength on ΔA, $\Delta \Phi$, and ΔM. Data that describe the wavelength dependence of the scattering properties of tissue are limited. However, the available literature[23,24] indicates that μ_s' of tissue (measured on forearm, leg, and head) decreases by less than 0.1% per nanometer change in wavelength. The absorption coefficients of the main tissue chromophores in the NIR (Hb, HbO$_2$, and water) change by up to 2% per nanometer. Therefore, by careful selection of the wavelength range to maximize $\Delta \mu_a$ changes, it is feasible that changes in μ_s' can be ignored.

(3) In the third experiment the absorption coefficient was estimated from attenuation, phase, and modulation depth measurements for different light source–detector distances. The literature[7–10] describes how the slope of attenuation and phase with distance is sufficient to derive both μ_a and μ_s'. For the solid phantom used in Subsection 3.B.3, slopes of 0.109 OD/mm and −0.0460 rad/mm were measured. Fitting μ_a and μ_s' [in Eqs. (1)–(3)] to these slopes provides μ_a and μ_s' values of 0.0134 mm^{-1} and 0.919 mm^{-1}, respectively. These values are in agreement with the true values of the phantom. The main advantage of the method suggested here is that the exact change in source–detector distance r does not need to be known. A possible optode design could incorporate a means to change r arbitrarily, e.g., by mechanically sliding the detector or the sensor or by optomechanical means over a few millimeters.

The main advantage of the method is its simplicity. First, no reference measurements are necessary and changes in A, Φ, and M are measured rather than absolute values. Furthermore, as a ratio Q_a, V_a, Q_r, or V_r is exploited, it is not essential to know the absolute magnitude of the changes (either $\Delta \mu_a$, $\Delta \lambda$, or Δr) that induce these ratios. Second, the aim of most biomedical applications is to derive chromophore concentrations, i.e., μ_a, whereas the scattering properties are of minor interest. Here, μ_a is directly derived from quantities (Q_a, V_a, Q_r, or V_r) that are largely insensitive to μ_s' and are to a good approximation dependent on μ_a only. Accordingly, μ_a can be read directly from plots such as those shown in Figs. 1(a), 2(a), 3(a), or 4(a), which can be created as lookup tables, and the requirement for data analysis is minimal. A single source–detector distance r is sufficient to derive μ_a from Q_a or V_a; this

might be advantageous for measurements of inhomogeneous media, such as tissue, for which different source or detector positions might be sensitive to different volumes of the medium.

The analysis of Section 2 describes that a variation in $\mu_s{}'$ by a factor of 5 alters the estimate of μ_a by only $\sim20\%$ if Q_a or Q_r is measured and by only a few percent for measurements of V_a or V_r. For most tissue types, the variability in $\mu_s{}'$ can be expected to be smaller than a factor of 2,[23] limiting the uncertainties in the estimate of μ_a to a few percent.

In the experiments on phantoms, described in Section 3, it was demonstrated that measurements of $\Delta A/\Delta\Phi$ or $\Delta\Phi/\delta M$ are equally able to derive μ_a. However, data measured in inhomogeneous media such as tissue are likely to require a more careful analysis. Arridge[25] and Arridge and Schweiger[26] have shown that different measurement functions such as A, Φ, or M have different sensitivities to spatial variations in μ_a, $\mu_s{}'$ that can be described in terms of photon measurement density functions. They demonstrate that intensity data are especially sensitive to changes of μ_a near the light source or the detector, i.e., close to the surface of the medium, whereas Φ is more susceptible to changes in deeper tissue layers. Φ and M probe similar volumes. These spatial sensitivity differences among A, Φ, and M are of no consequence in homogeneous media in which $\Delta A/\Delta\Phi$ and $\Delta\Phi/\delta M$ measurements derive the same μ_a. However, in inhomogeneous media, the differences might be substantial. For example, any changes in blood volume or oxygenation in a blood vessel close to the surface can induce a large attenuation change while Φ and M remain largely unaffected. Consequently, in highly inhomogeneous media, it might be advantageous to base μ_a estimations on $\Delta\Phi/\delta M$ measurements. Furthermore, in applications such as the Hb and HbO_2 monitoring of brain tissue, the deeper penetration depth of Φ and M might be required for reduced probing of the skin and skull of the head.

References

1. M. Cope and D. T. Delpy, "A system for the long-term measurement of cerebral blood and tissue oxygenation in newborn infants by near-infrared transillumination," Med. Biol. Eng. Comput. **26,** 289–294 (1998).

2. T. J. Farrell, B. C. Wilson, and M. S. Patterson, "The use of a neural network to determine tissue optical properties from spatially resolved diffuse reflectance measurements," Phys. Med. Biol. **37,** 2281–2286 (1992).

3. H. Lui, D. A. Boas, Y. Zhang, A. Yodh, and B. Chance, "Determination of optical properties and blood oxygenation in tissue using continuous NIR light," Phys. Med. Biol. **40,** 1983–1993 (1995).

4. S. J. Matcher, P. Kirkpatrick, K. Nahid, M. Cope, and D. T. Delpy, "Absolute quantification methods in tissue near-infrared spectroscopy," in *Optical Tomography, Photon Migration, and Spectroscopy of Tissue and Model Media: Theory, Human Studies, and Instrumentation*, B. Chance and R. R. Alfano, eds., Proc. SPIE **2389,** 486–495 (1995).

5. M. S. Patterson, J. D. Moulton, B. C. Wilson, K. W. Berndt, and J. R. Lakowicz, "Frequency-domain reflectance for the determination of the scattering and absorption properties of tissue," Appl. Opt. **30,** 4474–4476 (1991).

6. B. W. Pogue and M. S. Patterson, "Frequency-domain optical absorption spectroscopy of finite tissue volumes using diffusion theory," Phys. Med. Biol. **39,** 1157–1180 (1994).

7. S. Fantini, M. A. Franceschini, J. B. Fishkin, B. Barbieri, and E. Gratton, "Quantitative determination of the absorption spectra of chromophores in strongly scattering media: a light-emitting diode based technique," Appl. Opt. **33,** 5204–5213 (1994).

8. S. Fantini, M. A. Franceschini, and E. Gratton, "Semi-infinite-geometry boundary problem for light migration in highly scattering media: a frequency-domain study in the diffusion approximation," J. Opt. Soc. Am. B **11,** 2128–2138 (1994).

9. S. Fantini, M. A. Franceschini-Fantini, J. S. Maier, S. A. Walker, B. Barbieri, and E. Gratton, "Frequency-domain multichannel optical detector for noninvasive tissue spectroscopy and oximetry," Opt. Eng. **34,** 32–42 (1995).

10. J. B. Fishkin, P. T. So, A. E. Cerussi, S. Fantini, M. A. Franceschini, and E. Gratton, "Frequency-domain method for measuring spectral properties in multiple-scattering media: methemoglobin absorption spectrum in a tissuelike phantom," Appl. Opt. **34,** 1143–1155 (1995).

11. A. Duncan, T. L. Whitlock, M. Cope, and D. T. Delpy, "A multiwavelength, wideband, intensity modulated optical spectrometer for near infrared spectroscopy and imaging," in *Photon Migration and Imaging in Random Media and Tissues*, B. Chance, R. Alfano, and A. Katzir, eds., Proc. SPIE **1888,** 248–257 (1993).

12. B. J. Tromberg, L. O. Svaasand, T.-T. Tsay, and R. C. Haskell, "Properties of photon density waves in multiple-scattering media," Appl. Opt. **32,** 607–616 (1993).

13. S. J. Madsen, E. R. Anderson, R. C. Haskell, and B. J. Tromberg, "Portable, high-bandwidth frequency-domain photon migration instrument for tissue spectroscopy," Opt. Lett. **19,** 1934–1936 (1994).

14. M. Kohl, R. Watson, and M. Cope, "Determination of absorption coefficients in highly scattering media from changes in attenuation and phase," Opt. Lett. **21,** 1519–1521 (1996).

15. M. S. Patterson, B. Chance, and B. C. Wilson, "Time resolved reflectance and transmittance for the non-invasive measurement of tissue optical properties," Appl. Opt. **28,** 2331–2336 (1989).

16. S. Arridge, M. Cope, and D. T. Delpy, "The theoretical basis for the determination of optical pathlengths in tissue: temporal and frequency analysis," Phys. Med. Biol. **37,** 1531–60 (1992).

17. M. Sevick, J. Weng, M. Maris, and B. Chance, "Analysis of absorption, scattering, and haemoglobin saturation using phase modulation spectroscopy," in *Time-Resolved Spectroscopy and Imaging of Tissue*, B. Chance and A. Katzir, Proc. SPIE **1431,** 264–275 (1991).

18. T. J. Farrell, M. S. Patterson, and B. Wilson, "A diffusion theory model of spatially resolved, steady-state diffuse reflectance for the non-invasive determination of tissue optical properties in vivo," Med. Phys. **19,** 879–888 (1992).

19. C. F. Bohren and D. R. Huffman, *Absorption and Scattering of Light by Small Particles* (Wiley, New York, 1983), pp. 82–129.

20. M. Kohl, M. Essenpreis, and M. Cope, "The influence of glucose concentration upon the transport of light in tissue-simulating phantoms," Phys. Med. Biol. **40,** 1267–1287 (1995).

21. M. Firbank, M. Oda, and D. T. Delpy, "An improved design for a stable and reproducible phantom material for use in near-infrared spectroscopy and imaging," Phys. Med. Biol. **40,** 955–961 (1995).

22. R. Watson, M. Kohl, P. O'Brien, S. Lawrence, D. T. Delpy, and M. Cope, "Fetal brain oxygenation during labor studied by frequency domain spectroscopy," in OSA Trends in Optics and Photonics, *Biomedical Optical Sectroscopy and Diagnostics*, E. Sevick-Muraca and D. Benaron, eds. (Optical Society of America, Washington, D.C., 1996), Vol. 3, pp. 117–122.

23. S. J. Matcher, M. Cope, and D. T. Delpy, "*In vivo* measurements of the wavelength dependence of tissue-scattering coefficients between 760 and 900 nm measured using time-resolved spectroscopy," Appl. Opt. (to be published).

24. L. O. Svaasand, L. T. Norvang, E. J. Fiskerstrand, E. K. S. Stopps, M. W. Berns, and J. S. Nelson, "Tissue parameters determining the visual appearance of normal skin and port-wine stains," Lasers Med. Sci. **10,** 55–65 (1995).

25. S. R. Arridge, "Photon-measurement density functions. Part I: analytical forms," Appl. Opt. **34,** 7395–7409 (1995).

26. S. R. Arridge and M. Schweiger, "Photon-measurement density functions. Part 2: finite-element-method calculations," Appl. Optics **34,** 8026–8037 (1995).